Hindawi
International Journal of Aerospace Engineering
Volume 2022, Article ID 4231002, 13 pages
https://doi.org/10.1155/2022/4231002

Research Article

Experimental Investigation on Flow Characteristics of a Reverse-Flow Combustor

Ge Hu,[1] Jianzhong Li,[1] Wu Jin,[1] Jingzhou Zhang,[1] Li Yuan,[2] and Weikuo Zhai[3]

[1]*Key Laboratory of Aero-Engine Thermal Environment and Structure, Ministry of Industry and Information Technology, Nanjing University of Aeronautics and Astronautics, 29 Yudao St., Nanjing 210016, China*
[2]*School of National Defense Engineering, Army Engineering University of PLA, 88 Biaoying Rd., Nanjing, 210007 Jiangsu, China*
[3]*AECC Hunan Aviation Powerplant Research Institute, Zhuzhou 412002, China*

Correspondence should be addressed to Jianzhong Li; ljzh0629@nuaa.edu.cn

Received 20 December 2021; Revised 1 June 2022; Accepted 8 June 2022; Published 5 July 2022

Academic Editor: Linda L. Vahala

Reverse-flow combustor is widely used for small engines to overcome high speed shaft whirling problem and to provide a low frontal area. An experimental investigation was carried out to research the flow field characteristics of a reverse-flow combustor in this paper. Different aerodynamic conditions were studied using PIV to reveal the characteristics of both the nonreacting and reacting flow fields. The structure of the nonreacting flow field in the central section shows similarity as the total pressure loss coefficient increases. The penetrating depth, jet angle, recirculation zone position, and the flow streamlines are similar, while the velocity value of the flow field increases. The structure of the reacting flow field on the central section is different from that of nonreacting flow field, but the variation trend of the reacting flow field under different pressure loss coefficient is similar to that of the nonreacting flow field. By examining the nonreacting and reacting flow fields under the same total pressure loss conditions, marked differences were observed in the primary zone close to the swirler outlet. The relative motion between fuel injection, airflow, and combustion affects the flow field in this zone. The velocity with combustion is faster than that of the nonreacting flow because of the increased temperature and heat release.

1. Introduction

The study of combustors is particularly challenging due to the combined effects of thermodynamics and chemical reaction processes in the combustor. Typical combustor requirements include reliable ignition, stable combustion, small pressure loss, good quality of outlet temperature field, low exhaust emissions, compact structure, and lightweight construction [1–5]. The defining characteristics of a reverse-flow combustor are that the direction of the flame tube interior airflow is in the opposite direction to the inlet airflow. As well, the airflow through the combustor is subject to two 180° deflections. This feature integrates well with the centrifugal compressor, thereby reducing the combustor axis length significantly. Another benefit is a relative insensitivity to the inlet flow field and the production of a good quality of outlet temperature field. However, a common issue is unwanted fuel enrichment or the formation of a carbon area on the wall as a result of the small height of the flame tube channel. The compact reaction zone causes the fuel evaporation distance to be shortened, which affects combustion efficiency and stability. The study of reverse-flow combustors has attracted the attention of many scholars [6–14]. For example, Bharani et al. [9] showed that the flow characteristics and flow distribution of the jet holes of a reverse-flow combustor change when the flow characteristics of the outer annulus were altered. Additionally, the turbulence intensity level at the combustor outlet was not affected by the imposed inlet swirl. It can be found that most studies on the flow field are conducted by means of numerical simulation due to the compact structure of reverse-flow combustor. Based on the single-head reverse-flow combustor, this paper designed a reverse-flow combustor that can achieve optical

flow field measurement and explored the internal flow field characteristics by particle image velocimetry (PIV) experimental technique.

In order to further explore the combustor performance, it is important to understand the flow field characteristics in the combustor. Since the internal combustor airflow is strongly coupled and transient, advanced laser measuring techniques offer the capability to measure the combustor internal flow field under actual working conditions, improving the investigation quality. PIV is a noncontact measurement technique which offers full-field measurements without significant flow-field interference. Many researchers have studied combustor flow fields using PIV [15–20]. For example, the swirling flow inside a rectangular-shaped chamber was studied in [19]. The axial and radial velocity profiles over different planes were obtained by PIV to ascertain the effect of rectangular confinement inside the combustor. As well, the PIV technique was used to investigate the flow fields and fuel spray characteristics in an LPP combustor [20]. The results highlighted important changes in the flow field in the axial direction.

Compared with the nonreacting flow, the reacting flow is accompanied by complex processes of fuel atomization, vaporization, and mixing. As well, the flow field is highly coupled with chemical reactions. Therefore, investigations of the reacting flow field are necessary. Researchers have mainly used simulations or other experimental methods to investigate the influence of combustion on the flow field [21–28]. For instance, it showed that the reacting flow field could be predicted for perfectly premixed and partially premixed conditions using Large-Eddy Simulation (LES), and a good overall agreement was found between with the experimental and simulation data [21]. The changes of fluid dynamic features caused by combustion were studied using laser Doppler velocimetry (LDV), and the properties of the turbulent flow and their dependence on Reynolds number, swirl number, and chemical reactions were discussed [22]. As well, Chen and Liu [29] have introduced the application of PIV for this purpose and discussed its limitations in measuring the reacting flow field in combustion chambers. It showed that the flow field in the primary zone was different between the nonreacting flow field and the reacting flow field.

After the flow through the combustion chamber, the total pressure of the flow decreases in the flow process due to the viscosity of the gas, which is called the total pressure loss. The total pressure loss coefficient is defined as the ratio of the total pressure loss of the combustor to the average total pressure at the inlet of the combustor. The total pressure loss coefficient is a key parameter in the aerodynamic design of combustor, which has a significant impact on airflow penetration and mixing and thus on combustion performance. In this paper, PIV technique was used to measure the flow field in a reverse-flow combustor. The main research includes the influence of the total pressure loss coefficient on the nonreacting and reacting flow field was investigated; additionally, the influence of combustion on the flow field was investigated by comparing the nonreacting flow field with the reacting flow field under the same aerodynamic conditions.

2. Combustor Model and Experiment System

2.1. Reverse-Flow Combustor Structure. The fan-shaped reserve-flow combustor with a circumference of 20° shown in Figure 1(a) was investigated. The swirler consists of two radial blades and venturi tube; the outer diameter is 42 mm. A pressure atomizing nozzle with a cone angle of 80° (defined as the angle between the nozzle outlet and the two tangents of the spray grid) was used. The axis length and the height of the flame tube with no cooling hole are approximately 70 mm and 60 mm, respectively. The top and bottom jet holes were intentionally misaligned. Table 1 shows the parameters of jet holes. In order to create the optical measurement of the axial and radial plane of the combustor, sight windows 1 and 2 were arranged in the large elbow section and the sidewall surface of the combustor, respectively. Figure 1(b) shows a typical flow structure diagram of reverse-flow combustor. The outer and inner passage flow enter the flame tube; the top and bottom primary hole jets form the recirculation zone in the primary zone with the head airflow flowing through the swirler. It is helpful to stabilize ignition and combustion.

2.2. Experiment System. The experimental system in this paper consisted of the combustor model, air supply system, trace-particle generator, fuel supply system, ignition system, and the PIV system. A schematic of the system is shown in Figure 2. The airflow in the combustor was supplied by a root blower, and a vortex flowmeter and a valve were installed on the inlet pipeline. A pitot-pressure rake was installed before the inlet of the combustor to measure the total pressure of the inlet. The total pressure of the outlet was measured by a pitot-pressure rake at the outlet pipeline. The flow field was measured after the inlet and outlet total pressures met the test condition requirement by using a regulating valve. The flow in the combustor is a swirling flow with a three-dimensional structure. As the thickness (1 mm) of the two-dimensional PIV laser is very thin, the tracer particles cannot be guaranteed to move within the laser plane in a given time interval, which will cause measurement error. In order to reduce the measurement error, the actual time interval should be less than the estimated time interval [19]. The parameter of dt between two laser pulse was set to 2.0-4.0 μs, and the exposure time of two shooting was 1 ms in the experiment. Additionally, MgO particles with an average diameter of 10 μm were used as the tracer particles both in the nonreacting and reacting cases. In order to ensure a better distribution of the tracer particles in the combustor, the injection position of the tracer particles was kept far away from the combustor inlet in the axial direction. In this study, the PIV system was made up of a Bobcat B2041 digital camera with a maximum shooting frequency of 20 Hz and a maximum resolution of 2048 $\times$ 2048 pixels. An Nd: YAG double-pulse laser with a laser wavelength of 532 nm, maximum single-pulse energy of 200 mJ, and a maximum operating frequency of 15 Hz was used. A MicroPulse 725 synchronous controller was used to control the camera, the laser, and the image capturing board [30]. The PIV measurement parameters in the

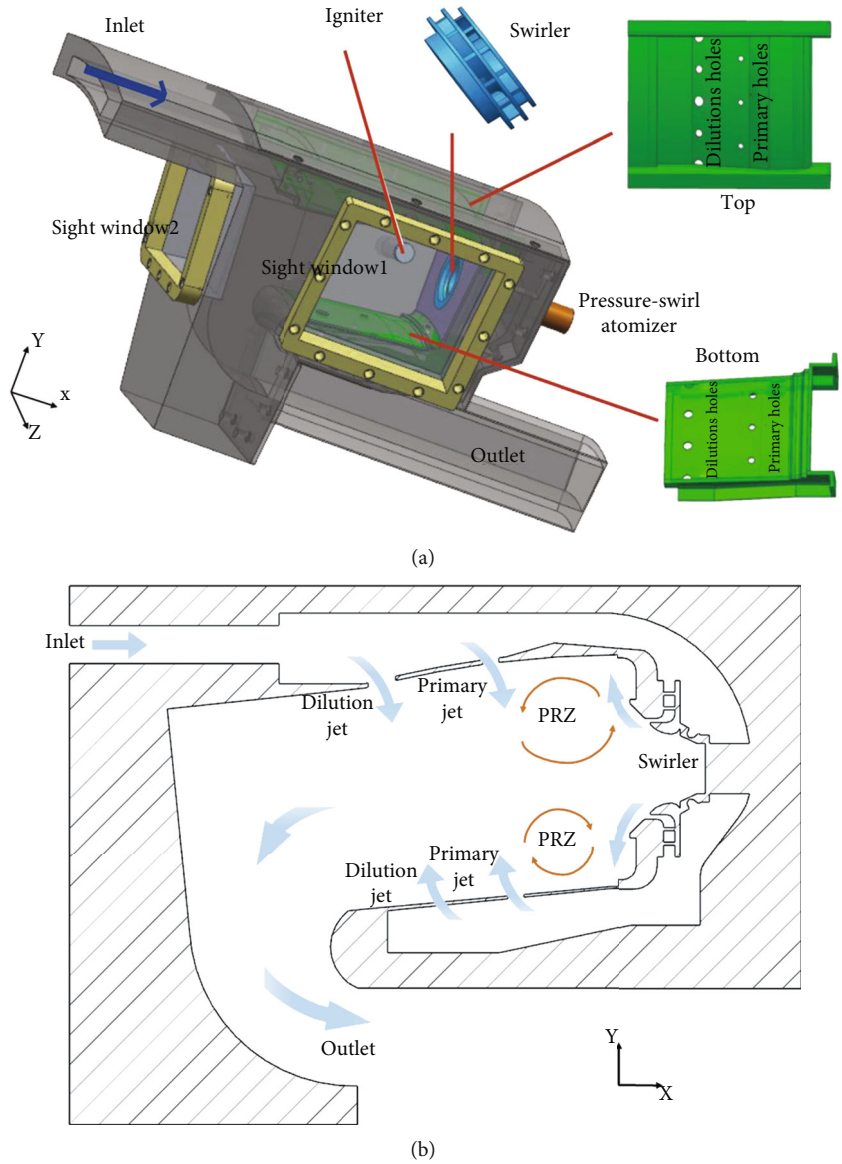

Figure 1: Schematic diagram of the reverse-flow combustor.

Table 1: Geometrical parameters of the jet holes ("○" refers to round hole, "△" refers to semicircle hole).

Parameters		Primary holes	Dilution holes
Arrangement	Top bottom	○ △—○—△	○ ○—○
Axial distance (mm)	Top bottom	36 63	25 48
Mass percentage of airflow		22%	48%

reacting cases were made to be as similar as possible to the nonreacting cases. However, in order to reduce the effect of flame and oil droplet reflection on the flow field measured by the PIV during combustion, a mechanical shutter and filter lens were installed on the camera. The time of exposure can be decreased by using a mechanical shutter, especially the exposure time of the second frame. This can reduce the effect of flame on the particle image, as shown in Figure 3. Figure 3(a) is the frame measured with no mechanical shutter, and Figure 3(b) is the frame measured with the mechanical shutter installed. It can be seen that the brightness of the flame in the frame is extremely strong when the mechanical shutter is not used. This brightness can seriously affect the interpretation of tracer particles by the PIV system. The brightness of the flame is obviously reduced when using the mechanical shutter. Therefore, the influence of the flame on the interpretation of tracer particles is greatly reduced. As well, an optical filter lens corresponding to a laser wavelength of 532 nm was added in front of the lens to reduce further the effect of flame and oil droplet reflection on the flow field measured by the PIV and maximize the accuracy of the results.

The nonreacting flow field and the reacting flow field of different sections of the combustor were measured. The

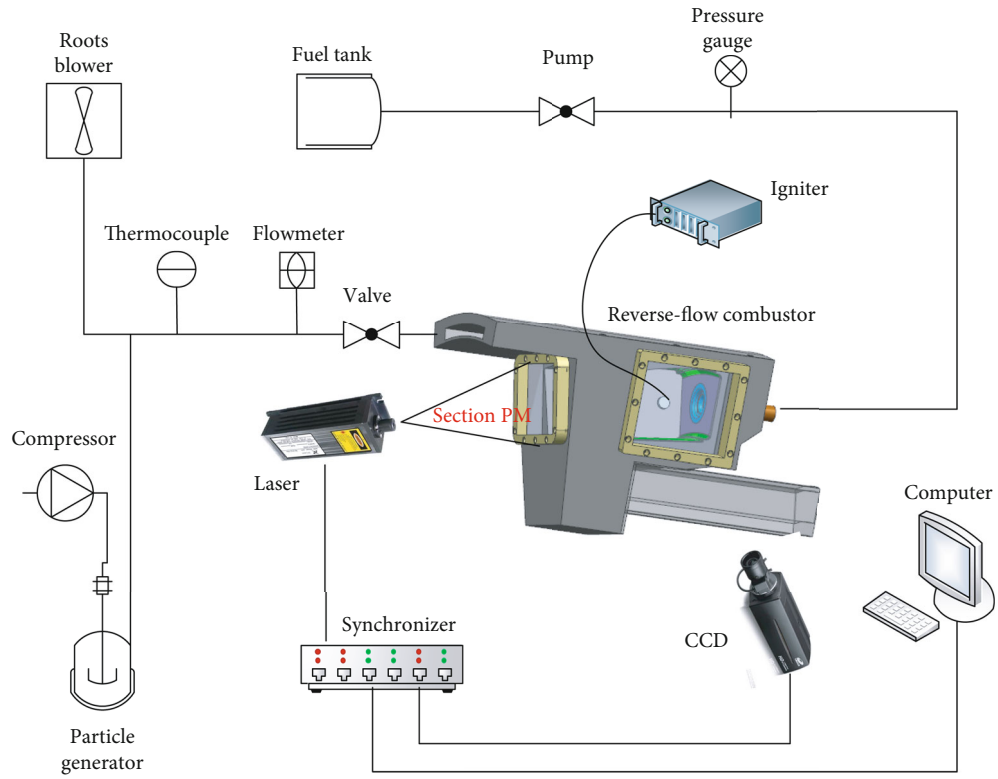

Figure 2: Schematic of the experimental system and the combustion chamber model.

(a) (b)

Figure 3: Example of a frame measured in different conditions: (a) frame measured with no mechanical shutter; (b) frame measured with a mechanical shutter.

measuring sections are shown in Figure 4(a). The axial cross section A is 10 mm downstream of the outlet of the swirler. Section B is the central meridional section of the combustor. Due to the vertical arrangement of the laser light path and the structure of the combustor, the effective acquisition window of the flow field on section B is outlined by the red dashed line in Figure 4(b). L denotes a line at a certain distance from the outlet of the swirler on section B. Specifically, $L1$, $L2$, $L3$, and $L4$ are 15 mm, 30 mm, 45 mm, and 60 mm, respectively. $L0$ is the central line. Here, the positive direction of the axial velocity is denoted as the positive direction along the X-axis. Similarly, the positive direction of radial velocity is the positive direction of Y-axis. Therefore, a positive axial velocity represents a reverse flow in the flame tube, and a negative axial velocity represents a downstream flow.

2.3. Postprocessing of Flow Field Results. The statistical independence of the number of transient nonreacting flow fields was analyzed before counting the flow field of the reverse-flow combustor. Figure 5 shows the comparison of the time-averaged axial velocities with different amounts of transient data (100, 200, and 300) along the central axis of the measurement section. It can be seen that there is a significant difference between the time-averaged velocity obtained by the statistics of the transient flow field of 100 frames and the statistical results of 200 and 300 frames, especially near the velocity peak. The statistical result of the 200 transient velocity fields is in good agreement with the statistical result of 300 frames at different axial positions. Therefore, 200 transient results are used for the analysis of time-averaged result.

3. Results and Discussions

The experiment was carried out at normal pressure and temperature (NPT). The inlet mass flow rates used in the combustor experimentally under different working conditions are shown in Table 2. According to the equation: $M_{\text{fuel}} = M_{\text{in}} \times \text{FAR}$, the fuel mass flow rate and fuel injection pressure under the corresponding working conditions can be obtained. The inlet mass flow rate of the combustor gradually increases with the increase of the total pressure loss coefficient.

Atomization characteristics of the centrifugal nozzle are shown in Figure 6. A Malvern spray analyzer was used to measure the Sauter mean diameter (SMD) at different locations; H represents the distance downstream of the nozzle outlet. High-speed photography was adopted to measure the atomization angle of the nozzle. The results indicate that the SMD gradually decreases with the distance from the

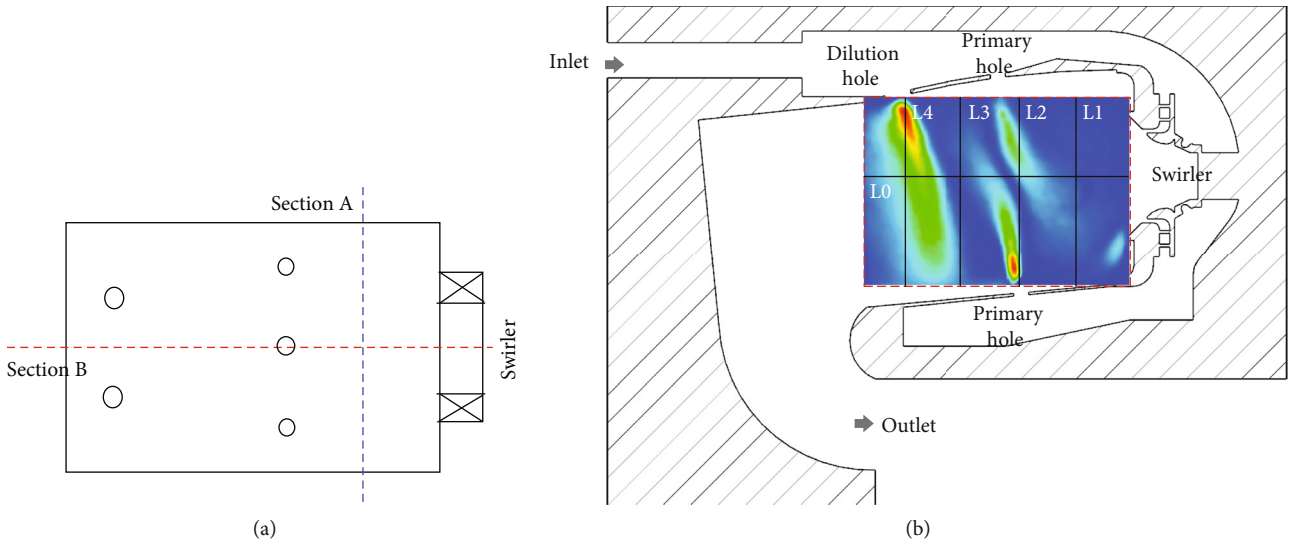

Figure 4: Schematic diagram of the measurement sections.

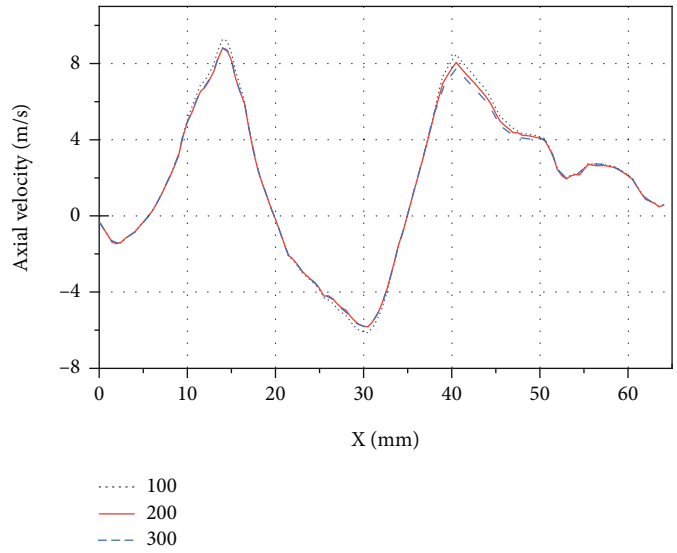

Figure 5: Effects of sample number on the profile of mean axial velocity.

Table 2: Operating parameters.

δ	Mass flow rate(g/s)	Fuel rate (g/s) FAR = 0.034	Fuel rate (g/s) FAR = 0.038
1%	7.5	0.26	0.28
3%	12.3	0.42	0.47
5%	16.3	0.55	0.62

outlet of the nozzle for the same atomizaiton pressure. As well, the SMD gradually decreases with the increase of atomization pressure at these three locations. When the atomization pressure is low, the SMD changes greatly, and the atomization angle of the nozzle changes dramatically, because the spray angle is not fully opened at low atomization pressure and the droplet atomization is unstable. In this paper, the atomization performance of the nozzle is relatively close in the experiment zone, so the influence of atomization performance differences on the experimental results is minimized.

Figures 7(a1), 7(b1), and 7(c1) show the nonreacting flow field in section B for δ values of 1%, 3%, and 5%, respectively; Figures 7(a2), 7(b2), and 7(c2) show the reacting flow field under an FAR of 0.034 for δ values of 1%, 3%, and 5%, respectively; Figures 7(a3), 7(b3), and 7(c3) show the reacting flow field under an FAR of 0.038 for δ values of 1%, 3%, and 5%, respectively. Examining the nonreacting flow fields shown in Figures 7(a1), 7(b1), and 7(c1), the results show that the deflection angle and penetration depth of the top and bottom jet holes under different δ values are uniform. As well, each of these flow fields has similar characteristics of inner and outer passage flow in the reverse-flow combustor. The top primary jet and bottom primary jet

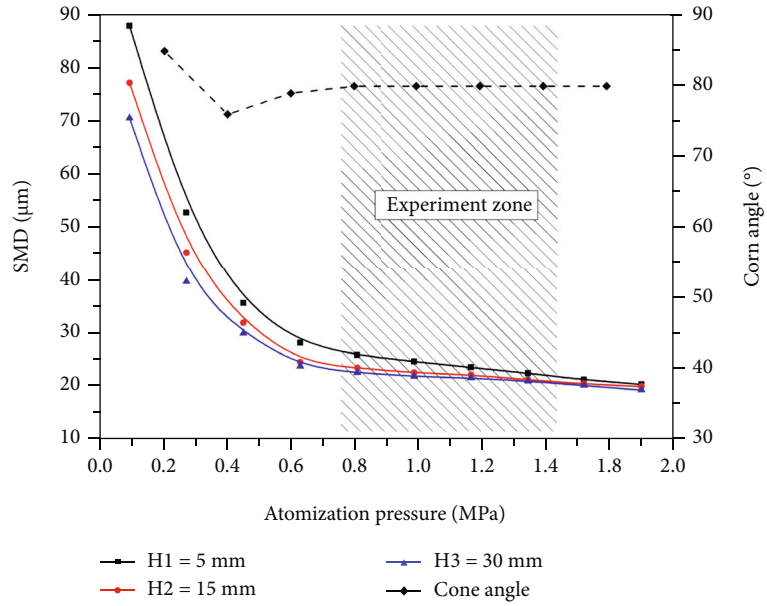

Figure 6: Spray nozzle atomizing properties.

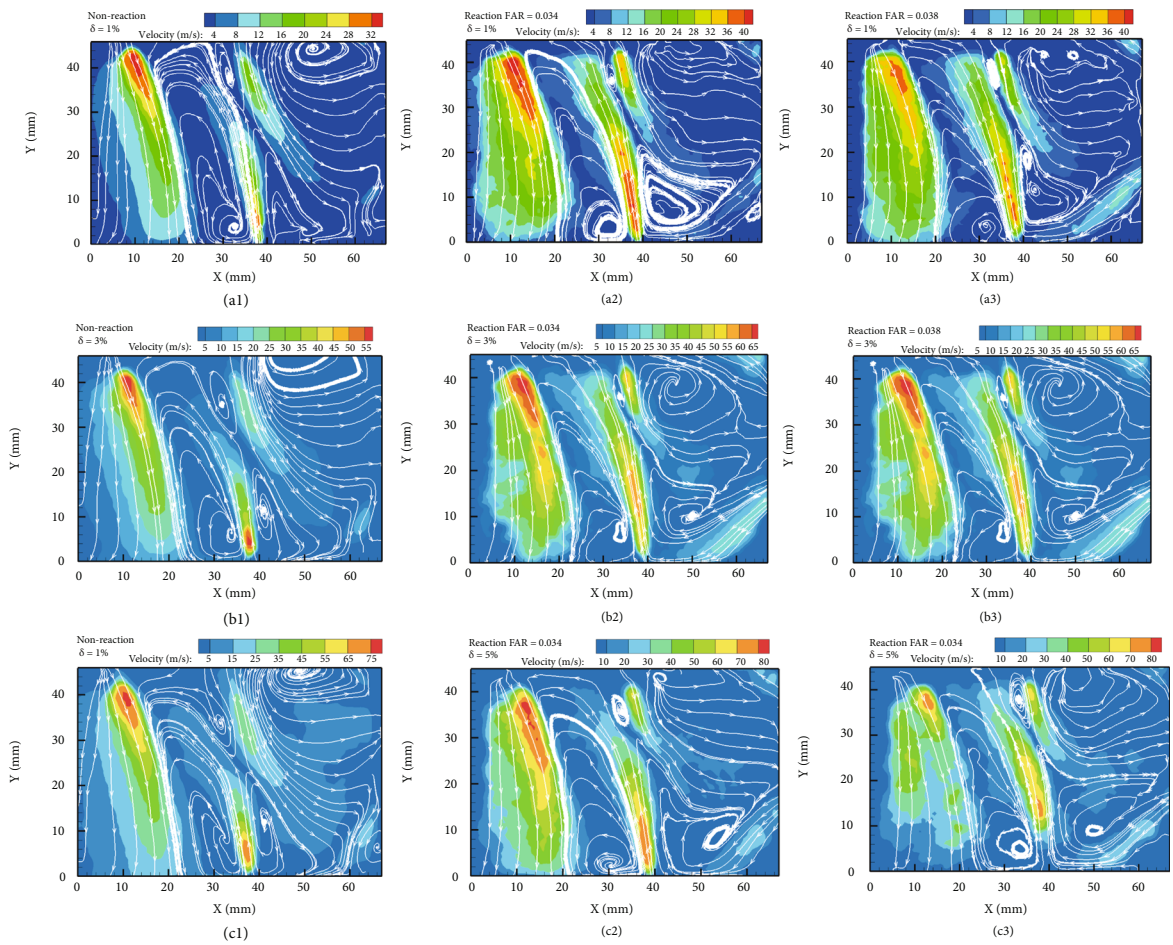

Figure 7: The flow field on central section B for different cases ((a) δ =1%, (b) δ =3%, (c) δ =5%; 1: nonreaction, 2: reaction, FAR = 0.034, 3: reaction, FAR = 0.038).

are staggered, and the top primary jet flows to the lower part of the head. Here, it forms a large recirculation zone in the upper primary zone with the head airflow flowing through the swirler. This process is helpful to stabilize ignition and combustion. The bottom primary jet flows to the secondary zone and forms two counterrotating recirculation zones close to the top/bottom liner in the secondary zone. The flow characteristics in this area are helpful for regulating the combustion structure and the fuel burn process. The velocity value everywhere in the combustor is increased with an increase in δ. Overall, the value of δ has little effect on the nonreacting flow field structure with the exception of the magnitude of the velocity field. Under a constant FAR, an examination of Figures 7(b1)–7(b3) and Figures 7(c1)–7(c3) shows that, for the reacting flow field, the original angle, deflection angle, and penetration depth of the top and bottom jet holes at different δ values are similar. As well, they all show the characteristics of the inner and outer passage flow of the reverse-flow combustor in all of these cases. Two strong jets can be observed in the head area. The angle between these two jets is essentially the same as the atomization cone, which is about 80°. The velocity value everywhere in the combustor increases with an increasing value of δ. This observation is consistent with conclusions found in the literature [31], which showed using PIV experiments and numerical simulations that the axial velocity increases and the radial velocity diverges with increased inlet Reynolds number. The difference in flow field structure is mainly close to the outlet of swirler. The mass fuel rate at the condition of $\delta = 3\%$ and FAR = 0.038 (Figure 7(b3)) is increased compared to the case shown in Figure 7(b2). In this case, the atomizing particle group failed to evaporate and combust quickly, thereby directing the flow field near the swirler outlet along the downstream direction. Fuel atomization performance was observed to be poorer when $\delta = 1\%$ and FAR = 0.038 (Figure 7(a3)), and the fuel mass flow rate is low; it causes that the magnitude of the velocity of the atomizing particle group is low, so the flow field near the swirler outlet also has a certain portion flowing in the downstream direction. It showed high fuel mass flow rate at the condition of $\delta = 5\%$ and FAR = 0.038 (Figure 7(c3)), but good atomization performance, strong combustion, heat dissipation, and fuel evaporation. So the region of downstream flow near the swirler outlet was very small. From the results, it can be concluded that δ has little effect on the reacting flow field structure with the exception of the velocity magnitude.

Compared with the cases of conditions 1, 2, and 3 under the same δ value, it shows that the nonreacting flow field structures are different from those of the reacting flow field. Although the jet has similar inner and outer passage flow characteristics for both the nonreacting and reacting states, the penetration depth of the bottom primary jet is significantly increased in the reacting state. As well, the bottom primary recirculation zone is affected by the top primary jet, causing the recirculation zone to be stretched and become larger. As well, the vortex nucleus of the top recirculation zone is moved. The peak airflow velocity in the reacting state is increased slightly compared to the nonreacting state. Due to the combustion, the resulting heat release and increased temperature reduce the density and cause the velocity of the airflow to increase. On the other hand, combustion causes more energy dissipation. As a result, the velocity gradient of the airflow increases, and the temperature rise of the airflow in the flame tube is significantly higher than that of the inner and outer passages. This causes the airflow density to become uneven, which results in a change in the jet depth and wake of the primary top and bottom holes. Compared to the nonreacting flow field, the subrecirculation zone upstream of the primary and dilution holes still exists. Additionally, the revolution of the recirculation zone is the same as that of the nonreacting state, but the subrecirculation zones are reduced in size. The flow field near the outlet of the swirler is noticeably different for the reacting and nonreacting flows. Two strong jets are found near the swirler outlet under the reacting state, and the angle between the two jets is basically the same as the atomization cone.

In Figure 8, the axial and radial velocity distributions at $L0$ in the nonreacting and the reacting states are shown under different δ. It can be seen that both the distributions of U and the distributions of V are similar under different δ in the three states. In all cases, the velocity magnitude increases with an increase in total pressure loss coefficient. This also shows that the change of δ does not affect the velocity distribution in the combustor but has an effect on the velocity magnitude [32]. This shows that the flow field in all cases is in the state of self-modeling [33]. Combined with the results shown in Figure 7, it can be concluded that a change of δ does not affect the structure of the nonreacting flow field and the reacting flow field significantly. The flow field characteristics are affected by the presence of combustion. Therefore, the subsequent investigation of the differences between the reacting and nonreacting flow fields is carried for δ value of 3%.

Figure 9 shows the distribution of tracer particles on section B in three different conditions obtained by PIV system. The distribution of tracer particles is relatively uniform, and the particle size is small (nonreaction state). The droplet without tracer particle in the reaction state mainly distributed in the area near the outlet of swirler. The distribution of droplet with tracer particle in the reacting state is different from that two conditions. And the particle size near the swirler outlet is larger than that in the downstream of the combustor. It can be found that the comtamination of droplet on tracer particle mainly occurs near the outlet of the swirler. As the droplet is rapidly burned, the comtamination of droplet on tracer particle at other downstream locations can be ignored.

Combined with the results shown in Figures 7 and 9, it can be concluded: the nozzle atomization dominates the fuel distribution near the outlet of the swirler. Conversely, the airflow transmission is less affected. When the distance from the swirler outlet is increased gradually, the fuel evaporation and airflow transmission are strengthened, and the fuel burns completely. Therefore, the flow field near the swirler outlet in the reacting state is different from that of the nonreacting state. The differences between these flows are affected by the fuel flow, atomization, and evaporation [34–36]. The secondary and dilution zones have several

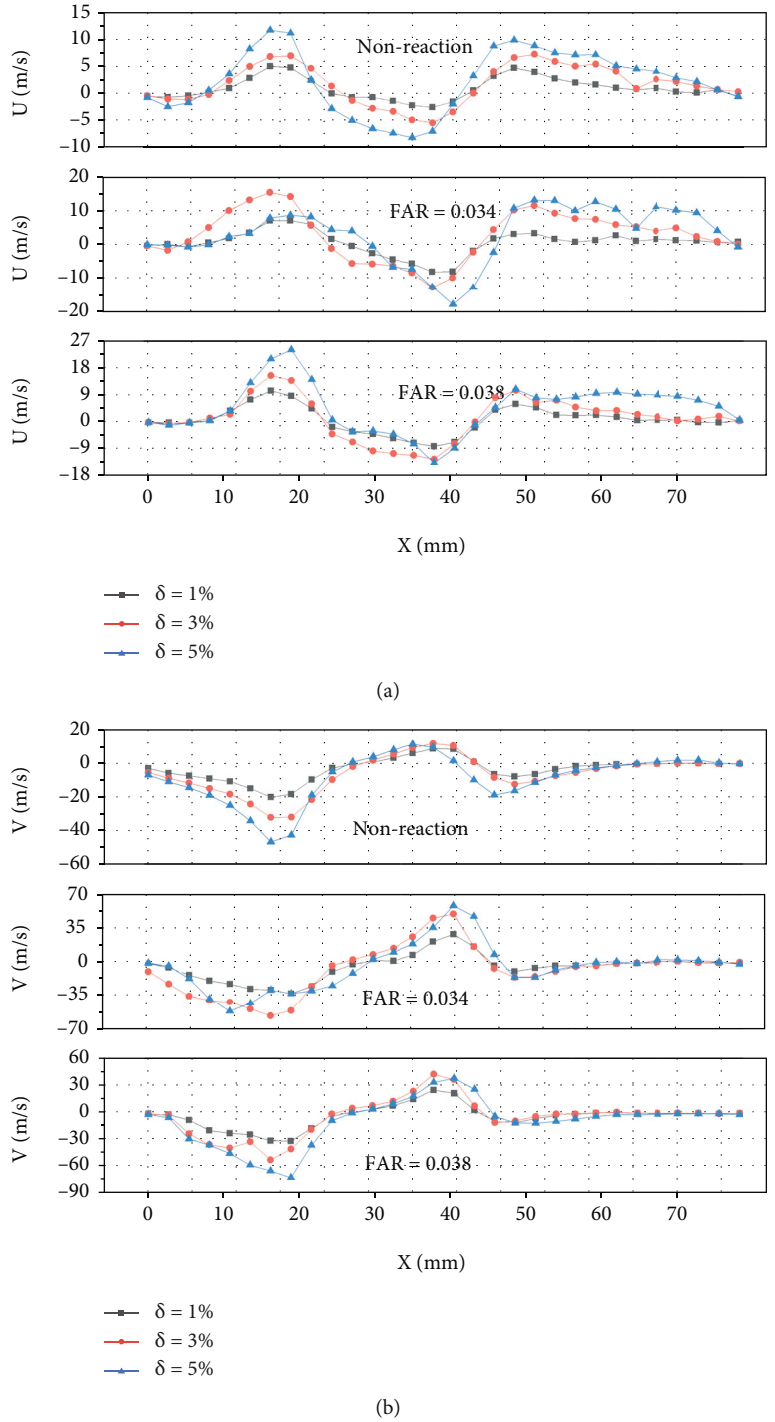

Figure 8: Profiles of velocity components on section B at $L0$: (a) axial velocity U; (b) radial velocity V.

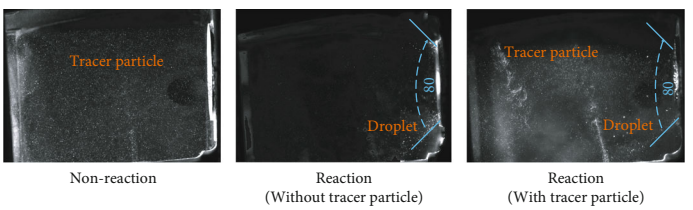

Figure 9: Particle image on section B in different conditions.

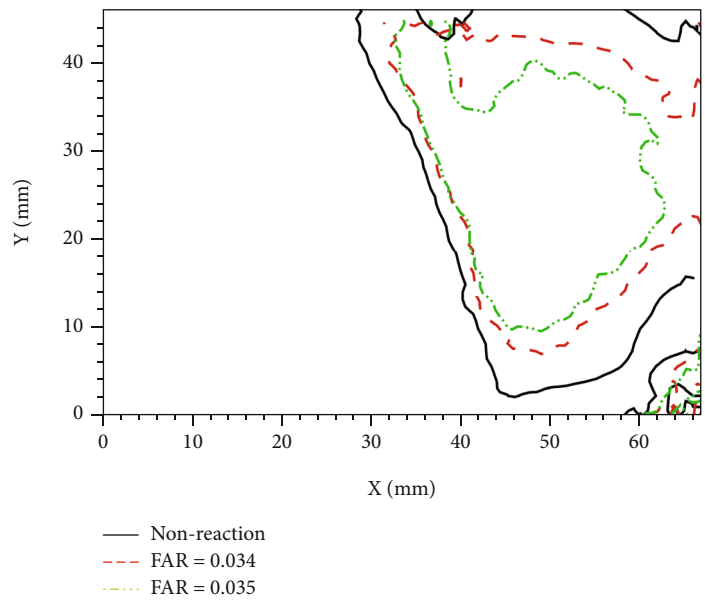

Figure 10: Boundaries of the primary recirculation zone in different cases.

similarities, and in both states, the dilution jets dictate the combustor exit velocity profiles.

The line where the axial velocity on section B is equal to 0 is used to represent the boundary of the recirculation zone. The structures of the PRZ under three different states are shown in Figure 10 for a total pressure loss coefficient of 3%. The results show that the PRZ in the nonreacting state is much larger. The primary stream in the combustor is squeezed by the high-speed atomized fuel. The subsequent combustion leads to heat release, and as a result, velocity gradient increased, and the airflow density is decreased. The area of the recirculation zone in the reacting case is significantly smaller than that in the nonreacting case. When FAR = 0.038, the PRZ is initially located approximately 5 mm downstream of the swirler outlet. The height of the PRZ when FAR = 0.038 is smaller than when FAR = 0.034. However, the tail location of the PRZ is essentially the same for both FAR = 0.038 and FAR = 0.034. The temperature rise of the airflow in the flame tube is significantly higher than in the inner and outer passages. This causes the airflow density to become uneven; then, the jet of the primary holes changes, which leads to the change of main flow structure. Although the combustion effects are slightly different in the two reaction cases. The height at the starting region of the PRZ is much smaller, and a region of fuel particles exists near the swirler outlet. This is because the fuel is not completely burned when FAR increases.

The profiles of velocity components when δ is 3% are shown in Figure 11. $L1$ is located in the primary zone. At $L1$, the velocity of U is negative at the position with a small Y value, but the amplitude is large in the two reacting cases. This result shows that the airflow flows in the downstream direction of the combustor. For the nonreacting case, U has a positive velocity value, indicating flow in the upstream direction. Additionally, the reversed flow is stronger in the middle area of the flow. The radial velocity V under the reacting state is located in the region of $Y < 8$ mm. Here, the radial velocity components are enhanced, and the flow is quite different from that of the nonreacting state. Compared with the distribution of U, the flow characteristics are similar to the fuel particle group near this area. The reacting flow field measured near this area is susceptible to the movement of atomized fuel. $L2$ is located near the primary hole. At this point, U and V have slightly different distributions in the nonreacting state and the reacting state. These differences are due to the influence of combustion on the primary hole jet. $L3$ is located in the secondary flow zone. Here, the velocity distributions in the nonreacting and reacting states are similar. $L4$ is located near the top dilution hole. When the upper dilution jet enters the flame tube, the jet flow is affected by the outer passage flow and has some characteristics similar to the outer passage flow. Therefore, the values of U and V both increase significantly and then decrease along the Y-axis. The velocity gradient of U and V in the reacting state is noticeably larger than the nonreacting state. In both states, the dilution jets distinctly dictate the combustor exit velocity profiles.

Contour plots of several pertinent quantities are presented here to illustrate the differences caused by the combustion. Figure 12 shows a contour of turbulence intensity and a velocity vector diagram on section B for nonreacting and reacting cases for a δ of 3%. The turbulence intensity is calculated as follows:

$$I = \frac{\sqrt{u'^2 + v'^2}}{\sqrt{u^2 + v^2}}, \quad (1)$$

where u is the mean axial velocity, v is the mean radial velocity, u' is the rms fluctuation of u, and v' is the rms fluctuation of v. The values were obtained by averaging 200 instantaneous flow field data points. The results show that the turbulence intensity in the recirculation zone downstream of the swirler is very low. As well, a high turbulence

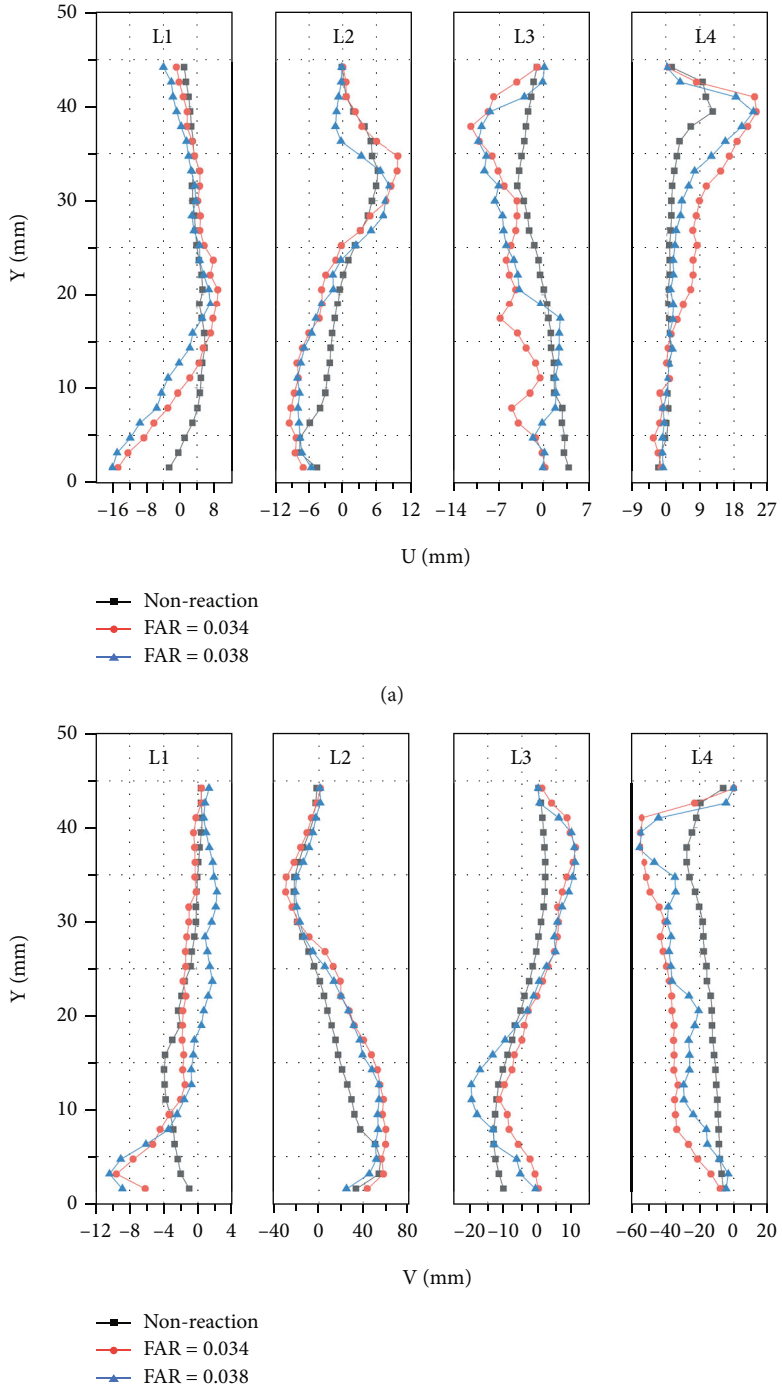

Figure 11: Profiles of velocity components on section B.

intensity area exists around the boundary of the recirculation zone. For the nonreacting case, the region with the highest turbulent intensity is near the wake of the recirculation zone. This is due to the large velocity gradient caused by the shear of the upper and lower primary hole jets. The turbulence intensity in the PRZ is low in both the reacting and nonreacting cases. It increases the residence time of fuel so that it can be fully burned. The effect of the high-speed atomized fuel on the flow is weakened with combustion and evaporation. As a result, the turbulence intensity is reduced along the downstream direction.

Profiles of the turbulence intensity and vorticity are shown in Figure 13. The vorticity is calculated from the two measured components of velocity using the relation: $\omega = \partial v/\partial x - \partial u/\partial y$. It can be find that turbulence intensity refers to the level of the flow velocity fluctuations, and vorticity is the curl of flow velocity. The vorticity distribution is very uneven and forms some locally concentrated strong

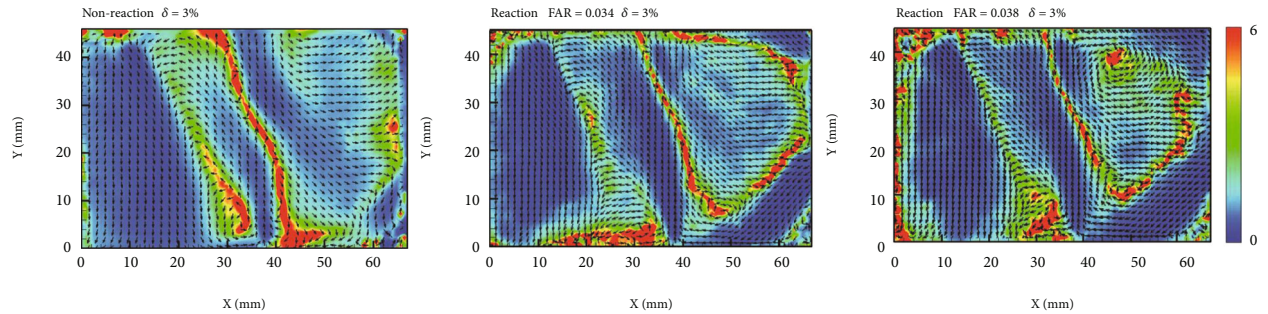

Figure 12: Contour plot of the turbulence intensity on section B.

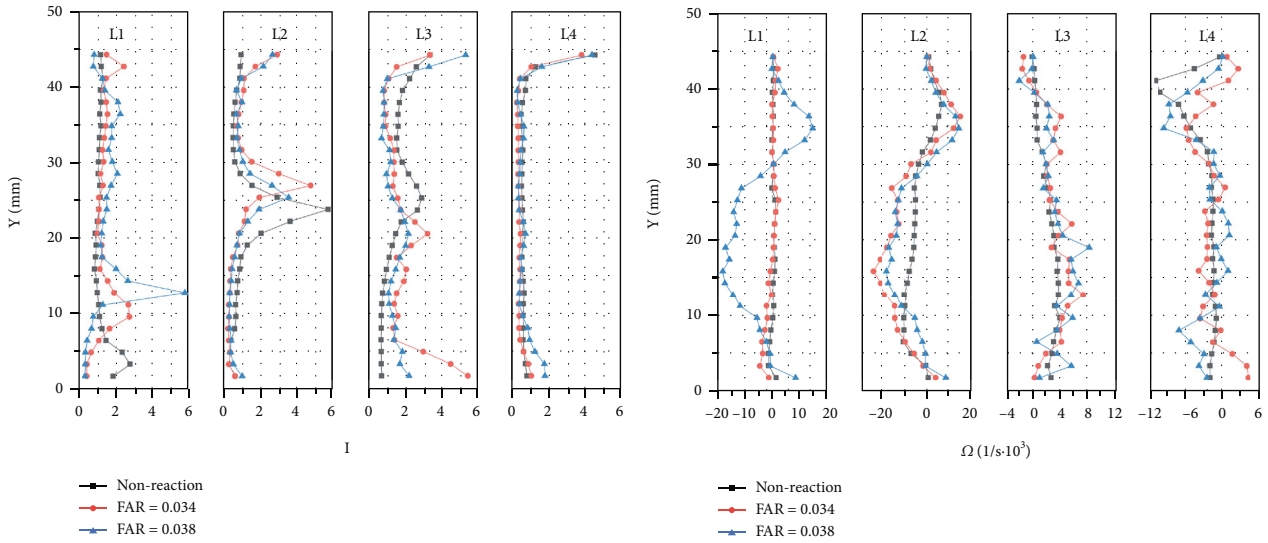

Figure 13: Profiles of turbulence intensity and vorticity at $L1$, $L2$, $L3$, and $L4$.

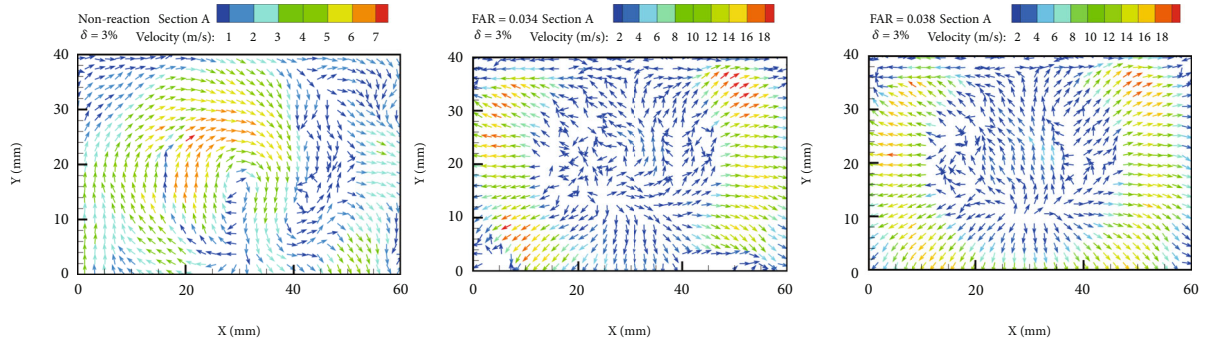

Figure 14: Velocity vector diagrams on section A for nonreacting and reacting cases.

vorticity areas. These areas can have a significant impact on the kinematic and dynamic properties of the entire flow field. It can be seen that the turbulence intensity at $L1$ is low for both the reacting and nonreacting cases. This is because $L1$ is located in the primary zone downstream of the swirler outlet. However, a crest near the lower boundary of the PRZ can be observed in the two reacting cases. The vorticity at $L1$ in the case of FAR = 0.038 is quite different from the other two cases. This is created because the atomizing fuel particle group has not yet evaporated and burned completely. As a result, the flow field near the swirler outlet is forced in the downstream direction. A crest in the turbulence intensity in both the nonreacting and reacting cases also exists at $L2$. The location of the crest in the reacting case is located higher than in the nonreacting case. As well, the turbulence intensity at the crest is slightly decreased. This further confirms the observation that the turbulence intensity near the boundary of the recirculation zone is strong. The vorticity at $L2$ in the reacting case is larger than that in the nonreacting state. The turbulence intensity and

vorticity at $L3$ and $L4$ in the reacting states are similar to that of the nonreacting case. However, the fluctuations are higher at these locations.

Velocity vector diagrams on section A for the different cases are shown in Figure 14. In the nonreacting case, a centrifugal force is generated by the strong tangential momentum of the airflow through the swirler and rotates the surrounding airflow. This rotation is related to the direction of the initial tangential momentum and depends on the structure of the swirler. In the present work, the airflow rotation is clockwise. The mainstream interacts with the primary hole jet and forms multiple circumferential reverse flow zones; these enhance the mixing effect of circumferential airflow in the combustor. In the two reacting cases, the structure of the velocity vector on section A is similar. In both cases, an obvious high-speed region of ring shape exists with the direction diverging outward from the centre. The peak velocity observed here is slightly faster for an FAR of 0.038. However, both reacting cases have significantly higher velocities compared to the nonreacting case. The flow structures are different in the reacting and nonreacting cases. Because the mass flow rate of the centrifugal nozzle increases as the FAR is increased, the velocity of the atomized fuel increases. The velocity of the atomized fuel is obviously larger than the airflow velocity for the nonreacting case. From the experimental results shown here, the flow field near the swirler outlet on section A in the reacting state is susceptible to the movement of atomized fuel.

4. Conclusions

In this paper, the flow field of a reverse-flow combustor was investigated experimentally. The experiment was carried out at NPT. The PIV technique was used to measure the flow field with and without combustion under different total pressure loss coefficients. The influence of total pressure loss coefficient on the flow field characteristics was studied. As well, the differences between the nonreacting and nonreacting flow field characteristics were studied. The conclusions list as follows:

The change of total pressure loss coefficient has little influence on the structures of both the nonreacting and reacting flow fields of the combustor. Specifically, the airflow direction, the recirculation zone locations, the deflection angle, and the penetration depth of the upper and lower jet holes remain unchanged with the increase of total pressure loss coefficient. However, in both the nonreacting and reacting states, the velocity magnitudes gradually increase with the increase of the total pressure loss coefficient. This shows that the flow field in all cases is in the state of self-modeling.

The presence of combustion has some influence on the flow field characteristics, which were observed by comparing the reacting and nonreacting cases. The most significant differences due to combustion occurred in the primary flow zone near the swirler outlet. The flow field near the swirler outlet is very susceptible to the movement of the atomized fuel in the reacting state. The secondary and dilution zones have several similarities in both the reacting and nonreacting cases. In both cases, the dilution jets dictate the combustor exit velocity profiles.

Nomenclature

CCD: Charge coupled device
PIV: Particle image velocimetry
FAR: Fuel/air ratio
PRZ: Primary recirculation zone
NPT: Normal pressure and temperature
δ: Total pressure loss coefficient
U: Axial velocity (m/s)
V: Radial velocity (m/s)
I: Turbulence intensity
ω: Vorticity.

Data Availability

The data used to support the findings of this study are available from the corresponding author upon request.

Conflicts of Interest

The authors declare that they have no conflicts of interest.

Acknowledgments

The authors would like to acknowledge support from the National Science and Technology Major Project (Grant Number 2017-III-0002-0026), the National Science and Technology Major Project (Grant Number 2019-III-0014-0058), the Natural Science Foundation of Jiangsu Province (Grant Number BK20190423), and the National Natural Science Foundation of China (Grant Number 51906106).

References

[1] H. Mongia, "Engineering Aspects of Complex Gas Turbine Combustion Mixers Part II: High T3," in *49th AIAA Aerospace Sciences Meeting including the New Horizons Forum and Aerospace Exposition*, Orlando, Florida, 2011.

[2] H. Mongia, "Engineering aspects of complex gas turbine combustion mixers part III: 30 OPR," in *9th Annual International Energy Conversion Engineering Conference*, 2011.

[3] H. Mongia, "Engineering aspects of complex gas turbine combustion mixers part V: 40 OPR," in *9th Annual International Energy Conversion Engineering Conference*, 2011.

[4] T. C. Lieuwen and V. Yang, *Gas Turbine Emissions: Contents*, vol. 38, Cambridge university press, 2013.

[5] D. R. Ballal and A. H. Lefebvre, "Ignition and flame quenching of flowing heterogeneous fuel-air mixtures," *Combustion & Flame*, vol. 35, pp. 155–168, 1979.

[6] K. S. Reddy, D. N. Reddy, and C. M. Varaprasad, "Experimental and numerical investigations of swirling flows in a reverse flow gas turbine combustor," in *37th AIAA Fluid Dynamics Conference and Exhibit*, 2007.

[7] K. S. Reddy and D. N. Reddy, "Combustion studies in swirling flows in a reverse flow gas turbine combustor using CFD," in *38th Fluid Dynamics Conference and Exhibit*, 2008.

[8] K. S. Reddy, D. N. Reddy, and C. M. V. Prasad, "CFD analysis of fuel distribution in concentric swirling flows in a reverse flow gas turbine combustor," in *ASME Turbo Expo 2006: Power for land, Sea, and Air*, 2006.

[9] S. Bharani, S. N. Singh, and D. P. Agrawal, "Effect of swirl on the flow characteristics in the outer annulus of a prototype reverse-flow gas turbine combustor," *Experimental Thermal & Fluid Science*, vol. 25, no. 6, pp. 337–347, 2001.

[10] S. Bharani, S. N. Singh, and D. P. Agrawal, "Effect of dump gap on velocity distribution and flow split in a prototype reverse-flow gas turbine combustor," *International Journal of Turbo & Jet Engines*, vol. 15, no. 2, 1998.

[11] M. H. Shojaeefard, K. Goudarzi, and K. Ariafar, "Numerical investigation of dump-gap's effect on velocity distribution and flow split in a model reverse-flow gas turbine combustor," in *21st Canadian Congress of Applied Mechanics(CANCAM 2007)*, 2007.

[12] X. Gao, F. Duan, S. C. Lim, and M. S. Yip, "Experimental and numerical study of flow structure and liner wall temperature in reverse flow combustor," in *International Heat Transfer Conference Digital Library*Begel House Inc.

[13] W. Xin, C. W. Peng, and S. Man, "Numerical study of performance of reverse flow combustor," in *IEEE Aerospace Conference*, 2016.

[14] L. Wang and T. Wang, "Investigation of the effect of perforated sheath on thermal-flow characteristics over a gas turbine reverse-flow combustor, part 2–computational analysis," *Journal of Thermal Science and Engineering Applications*, vol. 12, no. 4, pp. 1–11, 2019.

[15] R. F. Huang and F. C. Tsai, "Flow field characteristics of swirling double concentric jets," *Experimental Thermal & Fluid Science*, vol. 25, no. 3-4, pp. 151–161, 2001.

[16] Y. Zhao, J. Liang, and Y. Zhao, "Non-reacting flow visualization of supersonic combustor based on cavity and cavity-strut flameholder," *Acta Astronautica*, vol. 121, pp. 282–291, 2016.

[17] B. Jiang, Y. Jin, D. Liu et al., "Effects of multi-orifice configurations of the quench plate on mixing characteristics of the quench zone in an RQL-TVC model," *Experimental Thermal and Fluid Science*, vol. 83, pp. 57–68, 2017.

[18] Y. Jin, Y. Li, X. He et al., "Experimental investigations on flow field and combustion characteristics of a model trapped vortex combustor," *Applied Energy*, vol. 134, pp. 257–269, 2014.

[19] F. Vashahi, S. Lee, and J. Lee, "Experimental analysis of the swirling flow in a model rectangular gas turbine combustor," *Experimental Thermal & Fluid Science*, vol. 76, pp. 287–295, 2016.

[20] Y. Yan, L. Dang, Y. Deng, J. Li, and J. Zhao, "Experimental study of flow dynamics and fuel spray characteristics in Lean Premixed Prevaporized Combustor," *Fuel*, vol. 144, pp. 197–204, 2015.

[21] S. Gövert, D. Mira, J. B. Kok, M. Vázquez, and G. Houzeaux, "The effect of partial premixing and heat loss on the reacting flow field prediction of a swirl stabilized gas turbine model combustor," *Flow Turbulence & Combustion*, vol. 100, no. 2, pp. 503–534, 2018.

[22] C. Schneider, A. Dreizler, and J. Janicka, "Fluid dynamical analysis of atmospheric reacting and isothermal swirling flows," *Flow Turbulence & Combustion*, vol. 74, no. 1, pp. 103–127, 2005.

[23] G. Reichling, B. Noll, and M. Aigner, *Numerical Simulation of the Non-Reactive and Reactive Flow in a Swirled Model Gas Turbine Combustor*, Aiaa Computational Fluid Dynamics Conference DLR, 2015.

[24] M. Nikjooy, R. M. C. So, and R. E. Peck, "Modelling of jet- and swirl-stabilized reacting flows in axisymmetric combustors," *Combustion Science and Technology*, vol. 58, no. 1–3, pp. 135–153, 1988.

[25] M. R. Johnson, D. Littlejohn, W. A. Nazeer, K. O. Smith, and R. K. Cheng, "A comparison of the flowfields and emissions of high-swirl injectors and low- swirl injectors for lean premixed gas turbines," *Proceedings of the Combustion Institute*, vol. 30, no. 2, pp. 2867–2874, 2005.

[26] D. Lilley, "Swirling flows and lateral jet injection for improved mixing and combustion," in *49th AIAA Aerospace Sciences Meeting including the New Horizons Forum and Aerospace Exposition*, 2011.

[27] I. T. Nazzal and O. Ertunc, "Influence of turbulent flow characteristics on flame behaviour in diffuser combustors," *Energy*, vol. 170, pp. 652–667, 2019.

[28] R. C. Zhang, N. J. Bai, W. J. Fan, W. H. Yan, F. Hao, and C. M. Yin, "Flow field and combustion characteristics of integrated combustion mode using cavity with low flow resistance for gas turbine engines," *Energy*, vol. 165, pp. 979–996, 2018.

[29] F. Chen and H. Liu, "Particle image velocimetry for combustion measurements: applications and developments," *Chinese Journal of Aeronautics*, vol. 31, no. 7, pp. 1407–1427, 2018.

[30] J. Li, J. Chen, W. Jin, L. Yuan, and G. Hu, "The design and performance of a RP-3 fueled high temperature rise combustor based on RQL staged combustion," *Energy*, vol. 209, p. 118480, 2020.

[31] S. Dhanuka, J. Driscoll, and H. Mongia, "Instantaneous flow structures in a reacting gas turbine combustor," in *44th AIAA/ASME/SAE/ASEE Joint Propulsion Conference & amp; Exhibit*, 2008.

[32] J. Chen, J. Li, L. Yuan, and G. Hu, "Flow and flame characteristics of a RP-3 fuelled high temperature rise combustor based on RQL," *Fuel*, vol. 235, pp. 1159–1171, 2019.

[33] G. E. Hunt and G. K. Batchelor, "An introduction to fluid dynamics," *The Mathematical Gazette*, vol. 52, no. 380, p. 206, 1968.

[34] G. Li and E. J. Gutmark, "Effect of exhaust nozzle geometry on combustor flow field and combustion characteristics," *Proceedings of the Combustion Institute*, vol. 30, no. 2, pp. 2893–2901, 2005.

[35] B. Mohammad, S.-M. Jeng, and M. G. Andac, "Influence of the primary jets and fuel injection on the aerodynamics of a prototype annular gas turbine combustor sector," *Journal of Engineering for Gas Turbines and Power*, vol. 133, no. 1, 2011.

[36] H. Mak and S. Balabani, "Near field characteristics of swirling flow past a sudden expansion," *Chemical Engineering Science*, vol. 62, no. 23, pp. 6726–6746, 2007.